ISSN 1 746-7233, England, UK
World Journal of Modelling and Simulation
Vol. 12 (2016) No. 2, pp. 147-160

Magnetic effects on pulsatile flow of micropolar fluid through a bifurcated artery

D. Srinivasacharya* , G. Madhava Rao

Department of Mathematics, National Institute of Technology, Warangal, Telangana State, India, 506004

(*Received July 30 2015, Accepted January 23 2016*)

Abstract. Numerical simulations for MHD pulsatile flow in a bifurcated artery with mild stenosis in parent lumen in the presence of externally applied magnetic field are performed to investigate the blood flow phenomena on both sides of the apex (flow divider). Blood is considered as an electrically conducting micropolar fluid. The arteries forming bifurcation are taken to be symmetric about the axis of the artery and straight circular cylinders of restricted length. The governing equations are non-dimensionalized with suitable variables and coordinate transformation is used to make the regular boundary. The system of equations is solved numerically using the finite difference method. The variation of shear stress, flow rate and impedance near the flow divider with pertinent parameters are presented graphically. It has been noticed that shear stress, flow rate and impedance have been changing suddenly with all the parameters on both sides of the apex. This occurs because of the back flow of the streaming blood at the onset of the lateral junction and secondary flow near the apex in the daughter artery.

Keywords: micropolar fluid, bifurcated artery, mild stenosis, MHD, pulsatile flow

1 Introduction

Blood is treated to be one of the most important multi-component mixtures in the human body. This is composed of plasma, red blood cells and white blood cells, platelets, etc.. The flow of blood is the continuous circulation in the cardiovascular system and this process ensures the transportation of nutrients, hormones, metabolic wastes, etc.. throughout the body to maintain cell-level metabolism. The blood flow gives protection from microbial and mechanical harms. Typically the blood flow is laminar in healthy arteries, but the presence of abnormal flow conditions can promote the development of cardiovascular disease such as artherosclerosis. Vasoconstriction is the narrowing of the blood vessels resulting from contraction of the muscular wall of the vessels called stenosis. Once stenosis is formed and artery is bifurcated, the fluid mechanical, bio-mechanical and biochemical effects associated with the blood flow phenomenon are significantly changed. The formation of atherosclerotic plaque is more likely to be dependent on the geometry of the arteries. All the physiological properties of blood at the bifurcation of the artery are severely affected by different parameters. Several researchers have studied the blood flow in stenosed arteries of different geometries.

Many investigators studied the correlation between atherosclerosis and blood flow dynamics in the carotid artery assuming blood as an incompressible Newtonian fluid. It is well known that blood, being a suspension of cells, behaves like a non-Newtonian fluid at low shear rates and during its flow through narrow blood vessels. Gupta[9] investigated the flow field in the carotid artery considering fluid-structure interaction and the comparison between Newtonian and non-Newtonian fluid. Lee et al.[10] investigated the determination of the blood viscosity of non-Newtonian fluid using two constitutive models such as Casson and Herschel-Bulkley models. Nadeem et al.[14] studied blood flow through a tapered artery with stenosis assuming blood as a power law fluid. Tripathi et al.[23] considered the peristaltic flow of generalized Oldroyd-B fluids through

* *E-mail address*: dsc@nitw.ac.in.

a cylindrical tube under the influence of wall slip conditions. Nandakumar et al.[16] investigated the effects of percentage of stenosis and Reynolds number on pulsatile flow of a shear-thinning model for blood through a two-dimensional stenosed channel.

The theory of micropolar fluids introduced by Eringen [5] exhibits some microscopic effects arising from the local structure and micromotion of the fluid elements. Further, they can sustain couple stresses. The model of micro polar fluid represents fluids consisting of rigid randomly oriented (or spherical) particles suspended in a viscous medium where the deformation of the particles is ignored. The fluids containing certain additives, some polymeric fluids and animal blood are examples of micro polar fluids. Mekheimer and Mohamed [12] reported that the influence of the pulsatile flow of peristaltic motion of an incompressible conducting micropolar fluid through a porous medium in a channel are bounded with flexible walls. Misra et al.[13] presented that the amplitude of microrotation is highly sensitive to the changes in the magnitude of the suction velocity and the width of the micro channel and increase in the micropolar parameter give rise to a decrease in the amplitude of microrotation. Ellahi et al. [3] investigated the flow of unsteady and incompressible flow of non-Newtonian fluid through the composite stenosis by considering blood as a micropolar fluid and obtained an analytic solution. Ramana Reddy and Srikanth[20] discussed the blood flow through an overlapping clogged tapered artery in the presence of the catheter and revealed that shear stress at the wall is decreasing with increase in micropolar parameter and decrease in coupling number.

The application of magnetic fields play a vital role in the flow of blood in the human arterial system. MHD applications reduce the rate of flow of blood in the human arterial system, which is useful in the treatment of certain cardiovascular disorders. Several magnetic devices have been developed for drug carriers, cell separation, treatment of cancer tumor, etc.. Broad research work has been carried out on the bio-fluid mechanics in the presence of a magnetic field. On the other hand, heat transfer in blood has a huge number of applications in muscle and skin tissues, thermal therapy and other treatments. There have been a number of studies to examine heat transfer in blood vessels. Shit and Roy[21] investigated the effect of externally imposed body acceleration and magnetic field on the pulsatile flow of blood through an arterial system with stenosis. Sarifuddin et al.[2] developed a mathematical model of unsteady non-Newtonian blood flow together with heat transfer through constricted arteries. Srivastava[22] showed that the flow patterns in converging, diverging and non-tapered region are significantly influenced by the applied magnetic field and change in the inclination of the artery. Ellahi et al.[4] investigated the heat and mass transfer on a micropolar fluid of blood flow through a tapered stenosed artery of permeable walls. Fakour et al.[6] examined the laminar nanofluid flow and heat transfer in a channel with porous walls in the presence of transverse magnetic field using least square method. Majidian et al.[11] studied the laminar fluid flow in a semi-porous channel in the presence of transverse magnetic field using homotopy perturbation method and reported that velocity boundary layer thickness decrease with an increase in the value of the Reynolds number and Hartmann number. Nazir and Shafique[17] analyzed velocity, temperature, micro rotation and skin friction coefficient of the steady flow of a micropolar fluid, due to a stretching cylinder. Ramesh and Devakar[19] reported the influence of heat and mass transfer on the peristaltic flow of magnetohydrodynamic couple stress fluid flow through a homogeneous porous medium in a vertical asymmetric channel. Ponalagusamy and Selvi[18] presented the unsteady two-phase blood flow model in an artery with mild stenosis considering the effects of both heat transfer and magnetic field. Nadeem and Ijaz[15] obtained a closed form solution for temperature, slip velocity and velocity by using Cauchy Eulers method for mild stenosis case. Fakour et al.[7, 8] presented the study of heat transfer and flow of nanofluid in the presence of a magnetic field and micropolar fluid with chemical reaction in permeable channel.

The present article deals with the flow of an incompressible micropolar fluid through a bifurcated artery with mild stenosis. The variation of volumetic flow, impedance and shearing stress are analyzed for various values of micropolar parameter and half of the bifurcated angle.

2 Mathematical formulation

Consider the axially symmetric unsteady blood flow through a stenosed bifurcated artery with mild stenosis in the parent lumen. Let the magnetic field B_0 be externally applied normal to the direction of the blood flow. Assume that the arteries, forming bifurcations are symmetrical about the z-axes and are finite straight

circular cylinders. Further, it is assumed that curvature is introduced at the lateral junction and the flow divider so that the possibility of the presence of any discontinuity of the fluid flow leading to hypothetical flow separation zones can be eliminated. Let $(r,\ \theta,\ z)$ be the co-ordinates of any material point in a cylindrical polar coordinate system, of which z is treated to be the central axis of the parent artery. The fluid properties are considered to be constant, except for the density, so that the Boussinesq approximation is used.

Under the above assumptions, the governing equations of micropolar fluid flow may be written as follows

$$\frac{\partial \rho}{\partial t} + \rho(\nabla \cdot \overline{q}) = 0, \tag{1}$$

$$\rho(\frac{\partial \overline{q}}{\partial t} + (\overline{q} \cdot \nabla)\overline{q}) = -\nabla p + \kappa \nabla \times \overline{\nu} - (\mu + \kappa)\nabla \times \nabla \times \overline{q} + \rho g \beta_2 (T - T_\infty) - \sigma B_0^2 w, \tag{2}$$

$$\rho j(\frac{\partial \overline{\nu}}{\partial t} + (\overline{q} \cdot \nabla)\overline{\nu}) = -2k\overline{\nu} + \kappa \nabla \times \overline{q} - \gamma \nabla \times \nabla \times \overline{\nu} + (\alpha_1 + \beta_1 + \gamma)\nabla(\nabla \cdot \overline{\nu}), \tag{3}$$

$$\frac{\partial T}{\partial t} = \frac{k_0}{\rho c_p}\nabla^2 T + \frac{Q_1}{\rho c_p}(T - T_\infty), \tag{4}$$

where $\overline{\nu}$ is the microrotation vector, $\overline{q}$ is the velocity vector of blood flow and p is the fluid pressure, j and ρ and are microgyration parameter and the density of the fluid, T_∞ is the temperature on inner wall, c_p is the specific heat at constant pressure, k_0 is the thermal conductivity, Q_1 is the heat generation, β_2 is the volumetric expansion parameter, B_0 is the applied magnetic field. In addition to this, the material constants μ, κ, α_1, β_1 and γ satisfy the following inequalities[5].

$$\kappa \geq 0,\ 2\mu + \kappa \geq 0,\ 3\alpha_1 + \beta_1 + \gamma \geq 0,\ \gamma \geq |\beta_1| \tag{5}$$

The geometry of bifurcated artery with mild stenosis in parent lumen is represented with the following equations given by Chakravarty and Mandal[1]

$$R_1(z,t) = \begin{cases} aa_1(t) & 0 \leq z \leq d' \\ (a - \frac{4\tau_m}{l_0^2}(l_0(z-d') - (z-d')^2))a_1(t) & d' \leq z \leq d' + l_0 \\ aa_1(t) & d' + l_0 \leq z \leq z_1 \\ (a + r_0 - \sqrt{r_0^2 - (z-z_1)^2})a_1(t) & z_1 \leq z \leq z_2 \\ (2r_1 \sec\beta + (z - z_2)\tan\beta)a_1(t) & z_2 \leq z \leq z_{\max} \end{cases} \tag{6}$$

$$R_2(z,t) = \begin{cases} 0 & 0 \leq z \leq z_3 \\ (\sqrt{(r_0')^2 - (z - z_3 - r_0')^2})\ b_1(t) & z_3 \leq z \leq z_3 + r_0'(1 - \sin\beta) \\ (r_0'\cos\beta + z_4)\ b_1(t) & z_3 + r_0'(1 - \sin\beta) \leq z \leq z_{\max} \end{cases}, \tag{7}$$

where $a_1(t)$, $b_1(t)$ are given by

$$a_1(t) = 1 - (\cos(\omega t) - 1)k\ \exp(-k\omega t)$$
$$b_1(t) = \tfrac{1}{a_1(t)}$$

The radii of curvature at the lateral junction and the apex are r_0 and r_0' given by

$$r_0 = \frac{a - 2r_1\sec\beta}{\cos\beta - 1} \qquad \text{and} \quad r_0' = \frac{(z_3 - z_2)\sin\beta}{1 - \sin\beta}$$

where r_1 is the radius of the daughter artery, a is the radius of the parent artery at non-stenosed portion, β is the half of the bifurcation angle, l_0 is the length of the stenosis at a distance d' from the origin, τ_m is the maximum height of the stenosis at $z = d' + l_0/2$, $z_{\max}$ represents the maximum length of the bifurcated artery, z_1, z_2, z_3 are the location of the onset, offset of the lateral junction, flow divider respectively, these are defined as

$$z_2 = z_1 + r_0\sin\beta, z_3 = z_2 + q_1, z_4 = (z - z_3 - r_0'(1 - \sin\beta))\tan\beta$$

q_1 is a small number lying in between 0.1 and 0.5, this is defined for compatibility of the geometry.

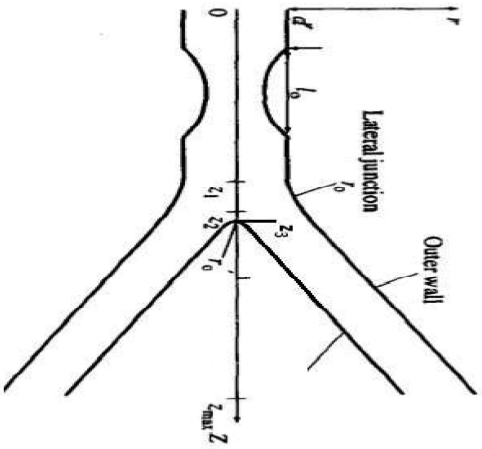

Fig. 1: Schematic diagram of stenosed bifurcated artery.

As the flow is symmetric about z-axis, all the variables are independent of θ. Hence, for this flow problem the velocity vector is given by $\overline{q} = (u(r,z), 0, w(r,z))$ and the microrotation vector is $\overline{\nu} = (0, \nu(r,z), 0)$. It can be assumed that the radial velocity is infinitesimally small and can be neglected for a small Reynolds number flow in an artery with mild stenosis. This implies that along the axial direction, the variation of all the flow characteristics are ignored except pressure. Therefore, the Eqs. (1) - (3) reduced to

$$\frac{\partial p}{\partial r} = 0, \tag{8}$$

$$\rho\frac{\partial w}{\partial t} = -\frac{\partial p}{\partial z} + \frac{\kappa}{r}\frac{\partial}{\partial r}(r\nu) + (\mu+\kappa)\frac{1}{r}\frac{\partial}{\partial r}\left(r\frac{\partial w}{\partial r}\right) + \rho g\beta_2(T-T_\infty) - \sigma B_0^2 w, \tag{9}$$

$$\rho j\frac{\partial \nu}{\partial t} = -2k\nu - \kappa\frac{\partial w}{\partial r} + \gamma\frac{\partial}{\partial r}\left(\frac{1}{r}\frac{\partial}{\partial r}(r\nu)\right), \tag{10}$$

$$\frac{\partial T}{\partial t} = \frac{k_0}{\rho c_p}\left(\frac{1}{r}\frac{\partial}{\partial r}(r\frac{\partial T}{\partial r})\right) + \frac{Q_1}{\rho c_p}(T-T_\infty). \tag{11}$$

The pulsatile pressure gradient present in the above equation is

$$-\frac{\partial p}{\partial z} = A_0 + A_1\cos(\omega t) \tag{12}$$

where A_0 is the constant pressure gradient, A_1 is the amplitude of systolic and diastolic pressure component and $\omega = 2\pi f_p$, f_p represents the frequency of the pulsatile flow.

The non-dimensional variables are given by[21]

$$\left.\begin{array}{l} r = a\widetilde{r}, w = \omega a\widetilde{w}, p = \omega\mu\widetilde{p}, z = a\widetilde{z}, \nu = \omega\widetilde{\nu}, t = \frac{\widetilde{t}}{\omega}, j = a^2\widetilde{j}, d = L\widetilde{d}, \\ \Theta = \frac{T-T_\infty}{T_w-T_\infty}, R_1(z) = a\widetilde{R}_1(\widetilde{z}), R_2(z) = a\widetilde{R}_2(\widetilde{z}),\ r_1 = a\widetilde{r}_1,\ z_1 = a\widetilde{z}_1 \end{array}\right\} \tag{13}$$

where a is characteristic length, ω is characteristic velocity and T_w is the temperature on the outer wall.

Using above non-dimensional variables in Eqs. (6) to (12) and dropping tildes, we have,

$$R_1(z,t) = \begin{cases} a_1 & 0 \le z \le d' \\ (1 - \frac{4\tau_m}{al_0^2}(l_0(z-d') - (z-d')^2)a_1 & d' \le z \le d'+l_0 \\ a_1 & d'+l_0 \le z \le z_1 \\ (1 + r_0 - \sqrt{r_0^2 - (z-z_1)^2})a_1 & z_1 \le z \le z_2 \\ (2r_1\sec\beta + (z-z_2)\tan\beta)a_1 & z_2 \le z \le z_{\max} \end{cases}$$

$$R_2(z,t) = \begin{cases} 0 & 0 \le z \le z_3 \\ (\sqrt{(r_0')^2 - (z - z_3 - r_0')^2})b_1 & z_3 \le z \le z_3 + r_0'(1-\sin\beta) \\ (r_0'\cos\beta + z_4)b_1 & z_3 + r_0'(1-\sin\beta) \le z \le z_{\max} \end{cases}$$

$$R_w^2 \frac{\partial w}{\partial t} = -\frac{\partial p}{\partial z} + \left(\frac{N}{1-N}\right)\frac{1}{r}\frac{\partial}{\partial r}(r\nu) + \left(\frac{1}{1-N}\right)\frac{1}{r}\frac{\partial}{\partial r}\left(r\frac{\partial w}{\partial r}\right) + \frac{G_r}{R_w^2}\Theta - H^2 w, \tag{14}$$

$$R_w^2 j(\frac{1-N}{N})\frac{\partial \nu}{\partial t} = -2\nu - \frac{\partial w}{\partial r} + \left(\frac{2-N}{m^2}\right)\frac{\partial}{\partial r}\left(\frac{1}{r}\frac{\partial}{\partial r}(r\nu)\right), \tag{15}$$

$$\frac{\partial \Theta}{\partial t} = \frac{1}{R_w^2 P_r}\frac{1}{r}\left(\frac{\partial(r\frac{\partial \Theta}{\partial r})}{\partial r}\right) + \frac{s\Theta}{R_w^2 P_r}, \tag{16}$$

where $P_r = \sqrt{\frac{\mu c_p}{k_0}}$is the Prandtl number, $G_r = \frac{\rho^2 g\beta_1 a^3(T_w - T_\infty)}{\mu^2}$ is the Grashof number, $H = B_0 a\sqrt{\frac{\sigma}{\mu}}$ is the Hartmann number, $R_w^2 = \frac{\rho a^2 \omega}{\mu}$ is the Womersley number, $s = \frac{Q_1 a^2}{k_0}$ is the Heat source parameter, $N = \dfrac{\kappa}{\mu + \kappa}$ is the micropolar coupling number $(0 \le N \le 1)$ and $m^2 = \dfrac{a^2\kappa(2\mu+\kappa)}{\gamma(\mu+\kappa)}$ is the micropolar parameter. It is to be noted from (14) and (15) that, when $N \to 0$ and $m \to \infty$ (i.e. $\kappa \to 0$ and $\gamma \to 0$) the system of equations represents to a classical Newtonian fluid model.

The respective non-dimensional boundary conditions are:

$$\left.\begin{array}{l} \dfrac{\partial w}{\partial r} = 0,\ \ \nu = 0,\ \ \Theta = 0 \ \text{ on } \ r = 0 \ \text{ for } \ 0 \le z \le z_3 \\ w = 0,\ \ \nu = 0,\ \ \Theta = 1 \ \text{ on } \ r = R_1(z) \ \text{ for all } \ z \\ w = 0,\ \ \nu = 0,\ \ \Theta = 0 \ \text{ on } \ r = R_2(z) \ \text{ for } \ z_3 \le z \le z_{\max} \\ w = w_0,\ \ \nu = 0 \ \text{ at initial time.} \end{array}\right\} \tag{17}$$

The influence of $R_1(z,t)$ and $R_2(z,t)$ can be transferred into the governing equations and boundary conditions by using the radial coordinate transformation given by Shit and Roy[21]

$$\xi = \frac{r - R_2}{R}, \tag{18}$$

where R(z,t) = $R_1(z,t)$ - $R_2(z,t)$, using (18) in Eqs. (14) to (16), we get

$$\begin{aligned} R_w^2\frac{\partial w}{\partial t} &= -\frac{\partial p}{\partial z} + \frac{N}{1-N}\left(\frac{1}{R}\frac{\partial \nu}{\partial \xi} + \frac{\nu}{\xi R + R_2}\right) \\ &+ \frac{1}{(1-N)R^2}\left[\frac{\partial^2 w}{\partial \xi^2} + \frac{R}{\xi R + R_2}\frac{\partial w}{\partial \xi}\right] + \frac{G_r}{R_w^2}\Theta - H^2 w \\ &+ R_w^2\frac{1}{R}\frac{\partial w}{\partial \xi}(\xi\frac{\partial R}{\partial t} + \frac{\partial R_2}{\partial t}), \end{aligned} \tag{19}$$

$$\begin{aligned} (\frac{1-N}{N})R_w^2 j\frac{\partial \nu}{\partial t} &= -\frac{1}{R}\frac{\partial w}{\partial \xi} + \frac{(2-N)}{m^2R^2}\left[\frac{\partial^2 \nu}{\partial \xi^2} - \frac{R^2}{\xi R + R_2)^2}\nu + \frac{R}{\xi R + R_2}\frac{\partial \nu}{\partial \xi}\right] \\ &-2\nu + (\frac{1-N}{N})R_w^2 j\frac{1}{R}\frac{\partial \nu}{\partial \xi}(\xi\frac{\partial R}{\partial t} + \frac{\partial R_2}{\partial t}), \end{aligned} \tag{20}$$

$$P_r R_w^2\frac{\partial \Theta}{\partial t} = \frac{1}{R^2}\frac{\partial^2 \Theta}{\partial \xi^2} + \frac{1}{R(\xi R + R_2)}\frac{\partial \Theta}{\partial \xi} + s\Theta + \frac{P_r R_w^2}{R}\left[\xi\frac{\partial R}{\partial t} + \frac{\partial R_2}{\partial t}\right]\frac{\partial \Theta}{\partial \xi}. \tag{21}$$

The wall motion of the bifurcated artery is shown in the last term on the right hand side of the above equations and the boundary conditions are transformed to the form

$$\left.\begin{array}{l} \dfrac{\partial w}{\partial \xi} = 0, \;\; \nu = 0, \;\; \Theta = 0 \;\text{ on }\; \xi = 0 \;\text{ for }\; 0 \le z \le z_3 \\ w = 0, \;\; \nu = 0, \;\; \Theta = 1 \;\text{ on }\; \xi = 1 \;\text{ for all } z \\ w = 0, \;\; \nu = 0 \;\; \Theta = 0 \;\text{ on }\; \xi = 0 \;\text{ for } z_3 \le z \le z_{\max} \\ w = w_0, \;\; \nu = 0 \;\text{ at initial time.} \end{array}\right\} \tag{22}$$

3 Method of solution

The reduced Eqs. (19) to (21) along with the boundary conditions (22) are solved numerically using finite-difference scheme. A three dimensional computational grid is considered. The stepping process is defined by $z_i = i\Delta z, i = 0, 1, \cdots, n$, $\xi_j = j\Delta\xi, j = 0, 1, \cdots, J$ and $t_k = k\Delta t, k = 0, 1, \cdots, m$ where Δz, Δt and $\Delta\xi$ are step lengths in the axial, time and radial directions respectively. If $w_{i,j,k}$ represents the value of the variable w at (z_i, ξ_j, t_k), then the derivatives are replaced by central difference approximations as shown below:

$$\begin{array}{l} \dfrac{\partial w}{\partial \xi} = \dfrac{1}{2}[\dfrac{w^{k+1}_{i,j+1} - w^{k+1}_{i,j-1}}{2\triangle\xi} + \dfrac{w^{k}_{i,j+1} - w^{k}_{i,j-1}}{2\triangle\xi}], \\ \dfrac{\partial^2 w}{\partial \xi^2} = \dfrac{1}{2}[\dfrac{w^{k+1}_{i,j+1} - 2w^{k+1}_{i,j} + w^{k+1}_{i,j-1}}{(\triangle\xi)^2} + \dfrac{w^{k}_{i,j+1} - 2w^{k}_{i,j} + w^{k}_{i,j-1}}{(\triangle\xi)^2}], \\ \dfrac{\partial w}{\partial t} = \dfrac{w^{k+1}_{i,j} - w^{k}_{i,j}}{\triangle t}, \end{array} \tag{23}$$

Similarly, we can write second order finite difference approximations for $\dfrac{\partial \nu}{\partial \xi}$, $\dfrac{\partial^2 \nu}{\partial \xi^2}$, $\dfrac{\partial \Theta}{\partial \xi}$, $\dfrac{\partial^2 \Theta}{\partial \xi^2}$, $\dfrac{\partial \nu}{\partial t}$ and $\dfrac{\partial \Theta}{\partial t}$.

Substituting (23) into (19) to (21), we get,

$$(a_1)^k_{i,j} w^{k+1}_{i,j-1} + (a_2)^k_{i,j} w^{k+1}_{i,j} + (a_3)^k_{i,j} w^{k+1}_{i,j+1} + (a_4)^k_{i,j} \nu^{k+1}_{i,j-1} + (a_5)^k_{i,j} \nu^{k+1}_{i,j} \tag{24}$$

$$+(a_6)^k_{i,j} \nu^{k+1}_{i,j+1} + (a_7)^k_{i,j} \Theta^{k+1}_{i,j} = (r_1)^k_{i,j} \tag{25}$$

$$(b_1)^k_{i,j} w^{k+1}_{i,j-1} + (b_2)^k_{i,j} w^{k+1}_{i,j+1} + (b_3)^k_{i,j} \nu^{k+1}_{i,j-1} + (b_4)^k_{i,j} \nu^{k+1}_{i,j} + (b_5)^k_{i,j} \nu^{k+1}_{i,j+1} = (r_2)^k_{i,j} \tag{26}$$

$$(c_1)^k_{i,j} \Theta^{k+1}_{i,j-1} + (c_2)^k_{i,j} \Theta^{k+1}_{i,j} + (c_3)^k_{i,j} \Theta^{k+1}_{i,j+1} = (r_3)^k_{i,j}, \tag{27}$$

where

$$\begin{array}{l} (a_1)^k_{i,j} = -\frac{R_w^2\, p(k)}{4\, R\, \triangle\xi} + \frac{1}{2\,(1-N) R^2\,(\triangle\xi)^2} - \frac{1}{4\,(1-N)\, R\, \triangle\xi\, (\xi R + R_2)}, \\ (a_2)^k_{i,j} = -\left[\frac{1}{(1-N)\, R^2\, (\triangle\xi)^2} + \frac{R_w^2}{\triangle t} + H^2\right], \\ (a_3)^k_{i,j} = \frac{R_w^2\, p(k)}{4\, R\, \triangle\xi} + \frac{1}{2\,(1-N) R^2\,(\triangle\xi)^2} + \frac{1}{4\,(1-N)\, R\, \triangle\xi\, (\xi R + R_2)}, \\ (a_4)^k_{i,j} = -(\frac{N}{4\,(1-N)\, R\, \triangle\xi}), \quad (a_5)^k_{i,j} = \frac{N}{(1-N)\,(\xi R + R_2)}, \\ (a_6)^k_{i,j} = (\frac{N}{4\,(1-N)\, R\, \triangle\xi}), \quad (a_7)^k_{i,j} = \frac{G_r}{R_w^2}, \\ (r_1)^k_{i,j} = -(a_1)^k_{i,j}\, w^k_{i,j-1} + (\frac{1}{(1-N)\, R^2\, \triangle\xi^2} - \frac{R_w^2}{\triangle t})\, w^k_{i,j} - (a_3)^k_{i,j}\, w^k_{i,j+1} \\ (a_4)^k_{i,j}\, \nu^k_{i,j-1} - (a_6)^k_{i,j}\, \nu^k_{i,j+1} + \frac{\partial p}{\partial z}, \end{array}$$

$$\begin{array}{l} (b_1)^k_{i,j} = \frac{1}{4\, R\triangle\xi}, \quad (b_2)^k_{i,j} = -\frac{1}{4\, R\triangle\xi}, \\ (b_3)^k_{i,j} = \frac{(2-N)}{m^2}\left(\frac{1}{2\, R^2\, (\triangle\xi)^2} - \frac{1}{4\, \triangle\xi\, R(\xi R + R_2)}\right) - \frac{(1-N)\, R_w^2\, j\, p(k)}{4\, N\, R\triangle\xi}, \\ (b_4)^k_{i,j} = -\left[2 + \frac{R_w^2\, (1-N)\, j}{N\, \triangle t} + \frac{2-N}{m^2\, R^2\, (\triangle\xi)^2} + \frac{2-N}{m^2\, (\xi R + R_2)^2}\right] \\ (b_5)^k_{i,j} = \frac{(2-N)}{m^2}\left(\frac{1}{2\, R^2\, (\triangle\xi)^2} + \frac{1}{4\, \triangle\xi\, R(\xi R + R_2)}\right) + (\frac{(1-N)\, R_w^2\, j\, p(k)}{4\, N\, R\, \triangle\xi} \\ (r_2)^k_{i,j} = -(b_1)^k_{i,j}\, w^k_{i,j-1} - (b_2)^k_{i,j}\, w^k_{i,j+1} - (b_3)^k_{i,j}\, \nu^k_{i,j-1} - \\ \left[\frac{R_w^2\, j\, (1-N)}{N\, \triangle t} - \frac{2-N}{m^2\, R^2\, (\triangle\xi)^2}\right] \nu^k_{i,j} - (b_5)^k_{i,j}\, \nu^k_{i,j+1} \end{array}$$

$$(c_1)^k_{i,j} = -\frac{p_r\ R_w^2\ p(k)}{4\ R\ \triangle\xi} + \frac{1}{2\ R^2\ (\triangle\xi)^2} - \frac{1}{4\ R\ \triangle\xi\ (\xi R+R_2)},$$
$$(c_2)^k_{i,j} = -\left[\frac{1}{R^2\ (\triangle\xi)^2} + \frac{p_r\ R_w^2}{\triangle t} - s\right],$$
$$(c_3)^k_{i,j} = \frac{p_r\ R_w^2\ p(k)}{4\ R\ \triangle\xi} + \frac{1}{2\ R^2\ (\triangle\xi)^2} + \frac{1}{4\ R\ \triangle\xi(\xi R+R_2)},$$
$$(r_3)^k_{i,j} = -(c_1)^k_{i,j}\ \Theta^k_{i,j-1} + \left[\frac{1}{2\ R^2\ (\triangle\xi)^2} - \frac{p_r\ R_w^2}{\triangle t}\right]\ \Theta^k_{i,j} - (c_3)^k_{i,j}\ \Theta^k_{i,j+1},$$

and

$$p(k) = \left(\xi^k_j \frac{\partial R^k_i}{\partial t} + \frac{\partial (R_2)^k_i}{\partial t}\right).$$

The Eqs. (24) to (27) along with the boundary conditions (22) are. are reduced into a block tri-diagonal system and it can be solved by block elimination method. The physical quantities to be discussed are the flow rate, shear stress and impedance for both parent and daughter arteries. The flow rate for both parent artery (Q_p) and daughter artery (Q_d) are determined by

$$Q_p = 2\pi R^k_i \left[R\int_0^1 \xi_j w^k_{i,j} d\xi_j + (R_2)^k_i \int_0^1 w^k_{i,j} d\xi_j\right], \tag{28}$$

$$Q_p = \pi R^k_i \left[R\int_0^1 \xi_j w^k_{i,j} d\xi_j + (R_2)^k_i \int_0^1 w^k_{i,j} d\xi_j\right]. \tag{29}$$

The resistance to the flow is defined as impedance, which can be obtained in the parent artery (λ_p) and daughter artery (λ_d) by using

$$(\lambda_p) = \left|\frac{z_3 \frac{dp}{dz}}{Q_p}\right| \ for\ z < z_3, \tag{30}$$

$$(\lambda_d) = \left|\frac{(z_{\max} - z_3)\frac{dp}{dz}}{Q_d}\right| \ for\ z \geq z_3. \tag{31}$$

The formula for shear stress along the inner and outer walls of the daughter artery is given by

$$\tau = \frac{1}{1-N}\frac{dw}{dr} + \frac{N}{1-N}v. \tag{32}$$

4 Results and discussion

For the computational domain, numerical solutions are computed by the grid size of $50 \times 40 \times 20$ for z, ξ and t respectively. The grid-independence study is made in order to obtain the results accurately. The necessary convergence of the results are achieved with the desired degree of accuracy. The results are illustrated through the Figs. 2- 14 followed by a complete discussion in order to substantiate the applicability of the present model. The aim of the current study is to investigate the flow characteristics of un-steady blood through the stenosed bifurcated artery under the action of an external magnetic field on the axial velocity by considering the effect of microrotation of blood cells. Theoretical results such as shear stress, volumetric flow rate and impedance for the blood flow are obtained in this analysis. The numerical solutions of all these physical quantities are shown graphically for different values of coupling number N, the bifurcation angle β, Hartmann number H, Heat source parameter s, Womesrley number R_w, Grashof number G_r and time t at different locations of the bifurcated artery. For better understanding of the analysis, following data has been used: $a = 0.005m$, $d' = 0.01m$, $l_0 = 0.005m$, $\beta = \frac{\pi}{10}$, $m = 10$, $r_1 = 0.51a$, $\tau_m = 2a$, $A_0 = 10\ N/m^3$, $A_1 = 0.2A_0\ N/m^3$, $t = 2sec$, $G_r = 2$, $H = 2$, $s = 1.5$, $p_r = 0.7$ and $R_w = 2$.

The effect of half of the bifurcated angle β and micropolar coupling number N on impedance in both sides of the apex are presented in Figs. 2a and 2b respectively. From Fig. 2a, it is observed that impedance is decreasing with the increase in the value of of β. From Fig. 2b it is seen that as the value of N increases impedance increases. Since in the limit $N \to 0$, Eqs. (2) and (3) reduce to the corresponding relations for a

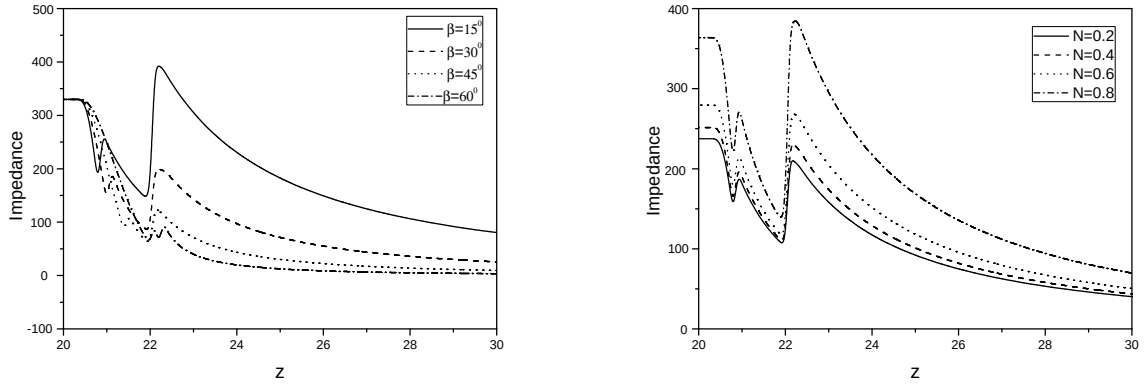

(a) (b)

Fig. 2: Variations of Impedance with (a) half of the bifurcated angle and (b) micropolar coupling number on both sides of the apex with fixed values of $H = 2$, $m = 10$, $s = 1.5$, $t = 2\ sec$, $P_r = 0.7$, $G_r = 2$ and $R_w = 2$.

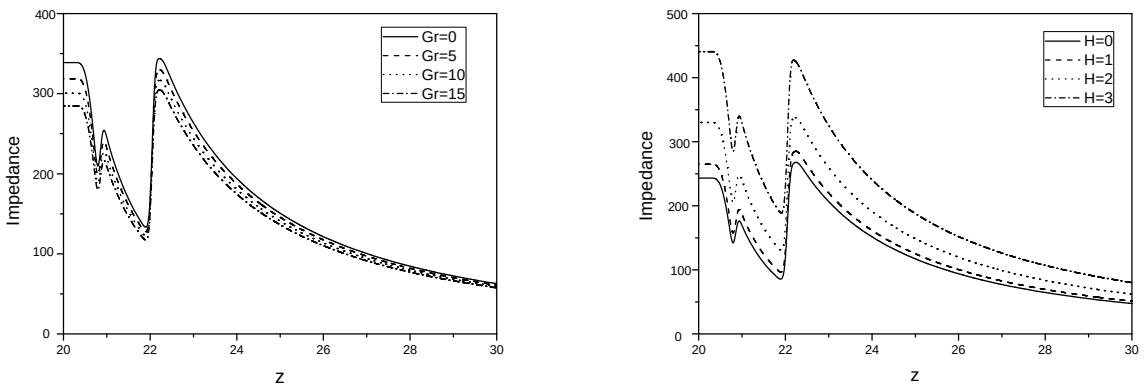

(a) (b)

Fig. 3: Variations of Impedance with (a) Grashof number and (b) Hartmann number on both sides of the apex with fixed values of $\beta = \frac{\pi}{10}$, $N = 0.75$, $m = 10$, $t = 2\ sec$, $s = 1.5$, $P_r = 0.7$ and $R_w = 2$.

viscous fluid, it is for one's observation, that the impedance in the case of micropolar fluid is more than that of viscous fluid. An increase in the value of N leads to an increase in the angular velocity indicating that an increase in vortex viscosity enhances the rotation of the micro-elements. Hence, the microstructure becomes significant in enhancing the impedance. Figs. 3a and 3b explore the effect of Grashof number G_r and magnetic parameter H on impedance in both sides of the apex. From 3a, it is noticed that the rise in the Grashof number G_r decreases the impedance on both sides of the apex. Similarly, 3b reveals that impedance is advancing with a rise in the value of magnetic parameter H on both sides of the apex. The variations of impedance with time t and Womersley number R_w are illustrated in Figs. 4a and 4b. It is noticed that increase in time t diminishes the impedance from Fig. 4a. Fig. 4b shows that the impedance is increasing with an increase in the value of R_w. In general, it is noticed from Figs. 2-4b that, the impedance is decreasing with an increase in the value of z, until inset of lateral junction, then a slight increase occurred suddenly, and after that a gradual decrease till the apex, and then a sudden increase is identified. This is because of the divergence of the blood flow at the bifurcation of the artery. Thereafter, it is found that the impedance is uniform till $z_{\max}$.

The variations of volumetric flow rate with the bifurcation angle β and coupling number N on both sides of the apex are presented in Fig. 5a and Fig. 5b. It is noticed from Fig. 5a that the flow rate is enhancing for

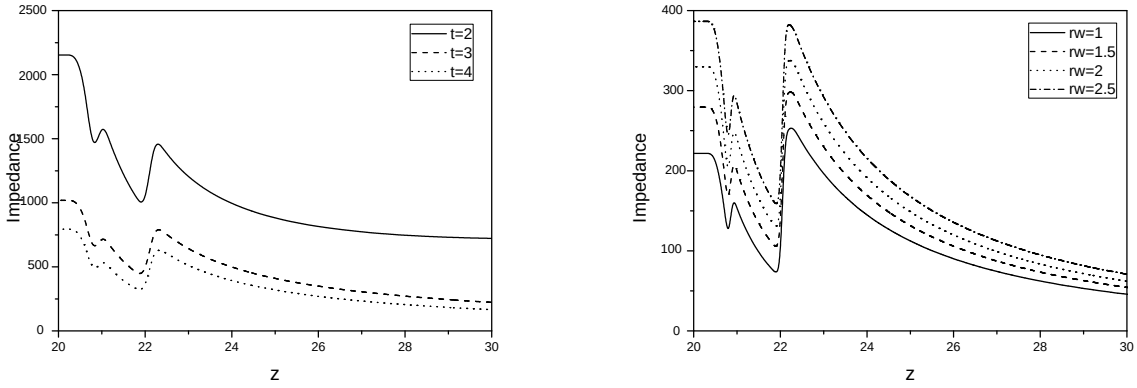

(a) (b)

Fig. 4: Variations of Impedance with (a) time and (b) Womersley number on both sides of the apex with fixed values of $\beta = \frac{\pi}{10}$, $N = 0.75$, $m = 10$, $s = 1.5$, $P_r = 0.7$, $G_r = 2$ and $H = 2$.

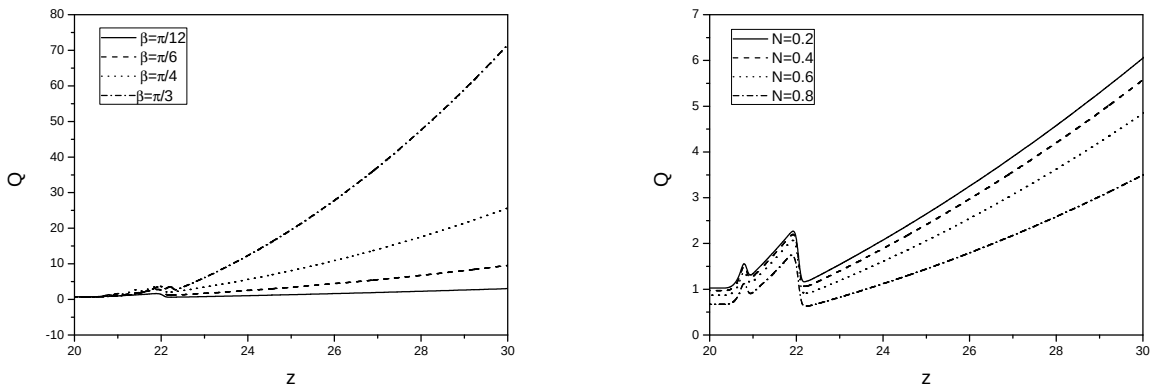

(a) (b)

Fig. 5: Variations of Volumetric flow rate with (a) half of the bifurcated angle and (b) micropolar coupling number on both sides of the apex with fixed values of $H = 2$, $m = 10$, $t = 2\ sec$, $s = 1.5$, $P_r = 0.7$, $G_r = 2$ and $R_w = 2$.

an increase in the value of β. The bifurcation angle declares to have an important role in the characteristics of the flow rate for the daughter artery. One can notice that for $\beta = 15^o$, the results representing flow rate are entirely negative due to forward flow and they become entirely positive for $\beta = 30^o$ and above due to flow reversal. From Fig. 5b it is observed that flow rate is decreasing with an increase in the value of N. The effect of micropolar rheology of streaming blood can be evaluated from the four lower curves, whereas the Newtonian model gives a higher flow rate. The decreased flow rate of a micropolar fluid is a consequence of the existence of particle microrotation and the relative rotation between microrotation and vorticity. The effects of G_r and H on the volumetric flow rate on both sides of the apex are shown in Figs. 6a and 6b. These figures show that the flow rate is increasing with a rise in the value of G_r and diminish in the value of H. It thus turns out that under the action of a magnetic field, the volume of blood flow can be controlled during surgeries. The influence of time t and R_w on flow rate on both sides of the apex is illustrated in Fig. 7a and Fig. 7b. It is observed that flow rate is increasing with an increase in the value of t and decrease in the value of R_w. From Figs. 5a - 7b, it is necessary to note that the flow rate is perturbed largely near to the apex in the parent artery due to the presence of back flow at the start of the flow divider. Flow rate is locally increasing

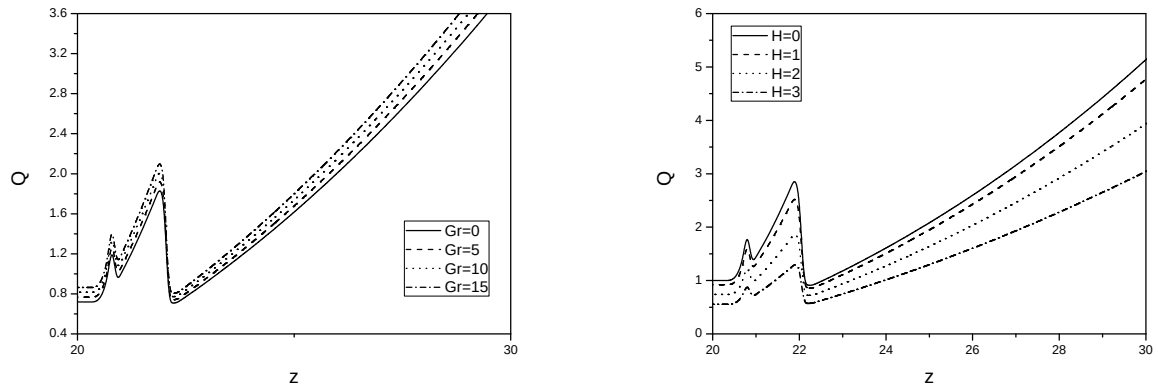

(a) (b)

Fig. 6: Variations of Flow rate with (a) Grashof number and (b) Hartmann number on both sides of the apex with fixed values of $\beta = \frac{\pi}{10}$, $N = 0.75$, $m = 10$, $t = 2$ *sec*, $s = 1.5$, $P_r = 0.7$ and $R_w = 2$.

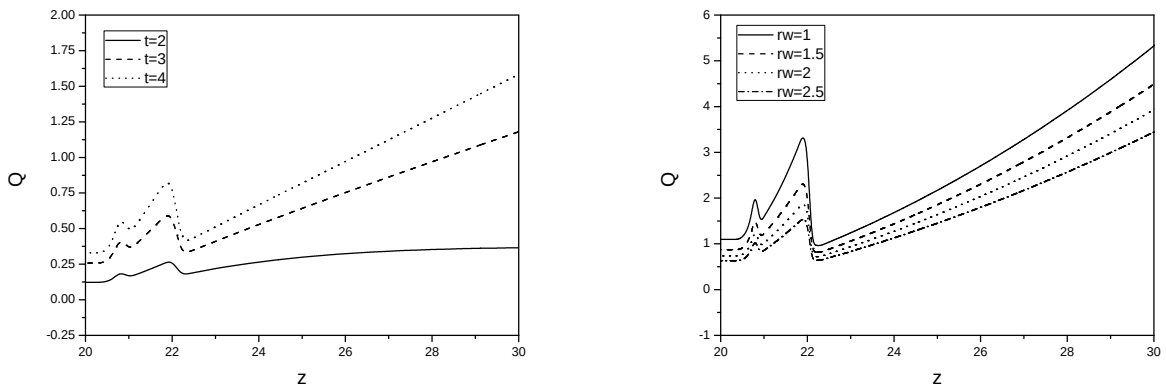

(a) (b)

Fig. 7: Variations of Flow rate with (a) time and (b) Womersley number on both sides of the apex with fixed values of $\beta = \frac{\pi}{10}$, $N = 0.75$, $m = 10$, $s = 1.5$, $P_r = 0.7$, $G_r = 2$ and $H = 2$.

till the onset of lateral junction, then a small decrease is identified and then increase until the apex. Thereafter, these profiles are found to be steady till $z_{\max}$.

The effect of β on shear stress along the inner and outer walls of the daughter artery is presented in Figs. 8a and 8b. It is noticed that, shear stress is decreasing along the inner wall and increases along the outer wall of the daughter artery with an increase in the value of β. The influence of G_r on shear stress along the inner and outer walls of the daughter artery is shown in Fig. 9a and Fig. 9b respectively. It is found that, shear stress is decreasing along the inner wall while increasing along the outer wall of the daughter artery with an increase in the value of G_r.

Figs. 10a and 10b explore the influence of H on shear stress along the inner and outer walls of the daughter artery. Shear stress is increased along the inner wall and decreased along the outer wall with an increase in the value of H. The effect of N on shear stress along the inner and outer walls of the daughter artery is presented in Figs. 11a and 11b. It is identified that, shear stress is decreasing along the inner wall and increase along the outer wall of the daughter artery with an increase in the value of N. The influence of R_w on shear stress along the inner and outer walls of the daughter artery are presented in Figs. 12a and 12b. It is noticed that, shear stress is rising along the inner wall and diminishes along the outer wall of the daughter artery with an advance in the value of R_w. The variations of shear stress with heat source parameter s along

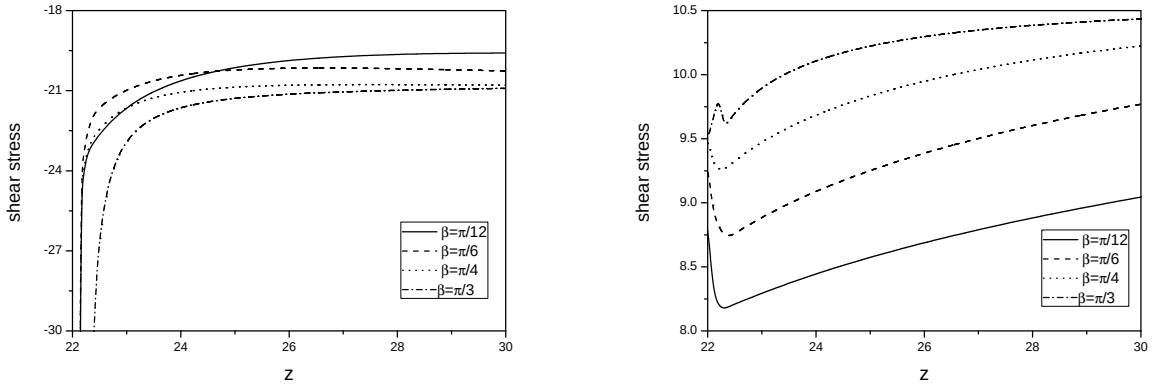

(a) (b)

Fig. 8: Influence of β on Shear stress along (a) the inner and (b) the outer walls of the daughter artery with fixed values of $H = 2$, $N = 0.75$, $m = 10$, $s = 1.5$, $t = 2\ sec$, $P_r = 0.7$, $G_r = 2$ and $R_w = 2$.

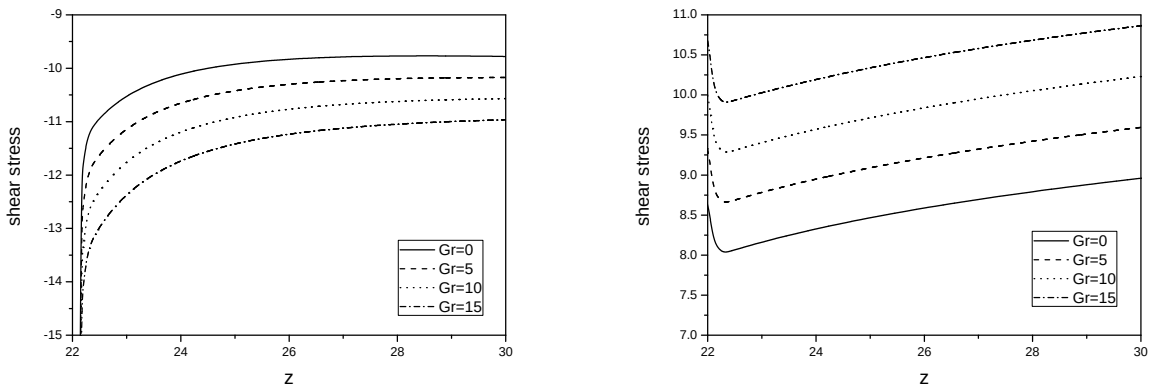

(a) (b)

Fig. 9: Influence of Grashof number on Shear stress along (a) the inner and (b) the outer walls of the daughter artery with fixed values of $H = 2$, $N = 0.75$, $m = 10$, $s = 1.5$, $t = 2\ sec$, $P_r = 0.7$, $\beta = \frac{\pi}{10}$ and $R_w = 2$.

the inner and outer walls of the daughter artery are illustrated in Fig. 13a and Fig. 13b. It is noticed that, shear stress is reducing along the inner wall and rising along the outer wall of the daughter artery with an increase in the value of s. The variations of shear stress with time (t) along the inner and outer walls of the daughter artery are shown in Fig. 14a and Fig. 14b. It is noticed that, shear stress is enhancing along the inner wall and diminishing along the outer wall of the daughter artery with an increase in the value of t.

5 Conclusions

The present results help us to understand, numerically as well as physically, the influence of N, β, G_r, H, t, and R_w on flow rate, shear stress and impedance of streaming blood flow through a bifurcated artery with mild stenosis. Here blood is treated as micropolar fluid. The following points have been concluded.

- The flow rate increases with increase values of β, G_r, t and decrease values of N, H, R_w both in parent and daughter arteries.
- The impedance decreases with increase values of β, G_r, t and increase values of N, H, R_w both in parent and daughter arteries.

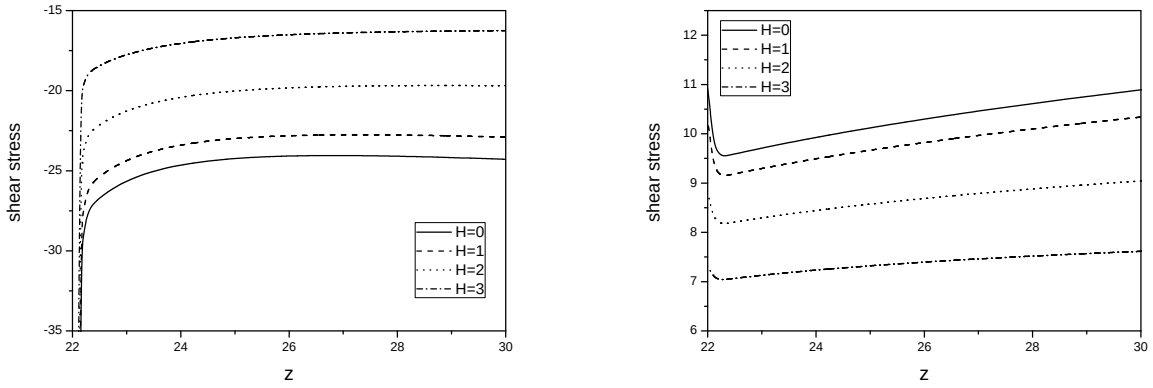

(a) (b)

Fig. 10: Influence of Hartmann number on Shear stress along (a) the inner and (b) the outer walls of the daughter artery with fixed values of $G_r = 2$, $N = 0.75$, $m = 10$, $s = 1.5$, $t = 2\ sec$, $P_r = 0.7$, $\beta = \frac{\pi}{10}$ and $R_w = 2$.

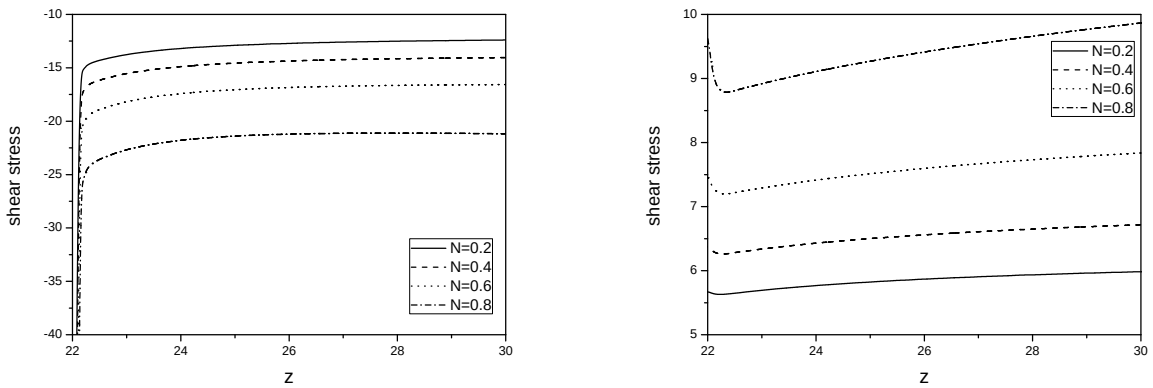

(a) (b)

Fig. 11: Influence of micropolar coupling number on Shear stress along (a) the inner and (b) the outer walls of the daughter artery with fixed values of $H = 2$, $G_r = 2$, $m = 10$, $s = 1.5$, $t = 2\ sec$, $P_r = 0.7$, $\beta = \frac{\pi}{10}$ and $R_w = 2$.

- The shear stress increases with increase in the values of H, R_w, t, decrease in the values of β, G_r, N, s along the inner wall of the daughter artery and shear stress increases with increase values of β, G_r, N, s, decrease values of H, R_w, t along the outer wall of daughter artery.

References

[1] S. Chakravarty, P. Mandal. An analysis of pulsatile flow in a model aortic bifurcation. *International journal of engineering science*, 1997, **35**(4): 409–422.

[2] S. Chakravarty, P. Mandal, et al. Heat transfer to micropolar fluid flowing through an irregular arterial constriction. *International Journal of Heat and Mass Transfer*, 2013, **56**(1): 538–551.

[3] R. Ellahi, S. Rahman, et al. A mathematical study of non-newtonian micropolar fluid in arterial blood flow through composite stenosis. *Applied Mathematics & Information Sciences*, 2014, **8**(4): 1567.

[4] R. Ellahi, S. Rahman, et al. Influence of heat and mass transfer on micropolar fluid of blood flow through a tapered stenosed arteries with permeable walls. *Journal of Computational and Theoretical Nanoscience*, 2014, **11**(4): 1156–1163.

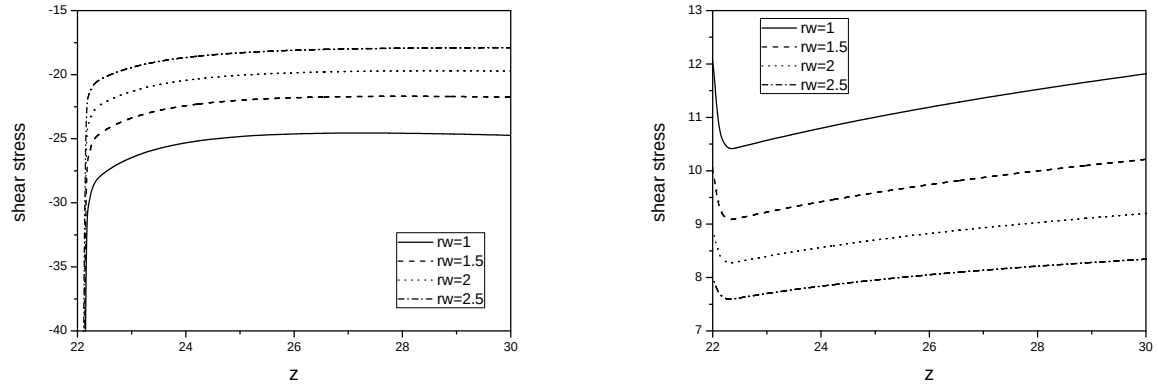

(a) (b)

Fig. 12: Influence of Womersley number on Shear stress along (a) the inner and (b) the outer walls of the daughter artery with fixed values of $H = 2$, $N = 0.75$, $m = 10$, $s = 1.5$, $t = 2\ sec$, $P_r = 0.7$, $\beta = \frac{\pi}{10}$ and $G_r = 2$.

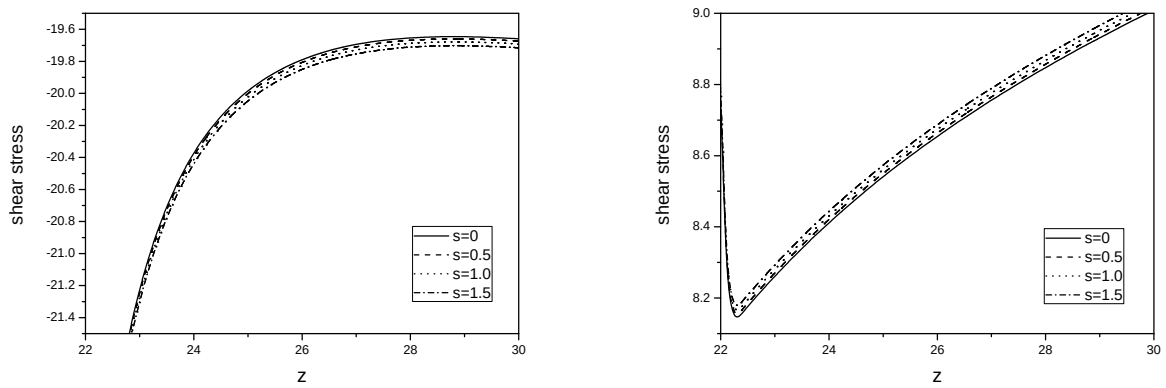

(a) (b)

Fig. 13: Influence of Heat source parametr on Shear stress along (a) the inner and (b) the outer walls of the daughter artery with fixed values of $H = 2$, $N = 0.75$, $m = 10$, $G_r = 2$, $t = 2\ sec$, $P_r = 0.7$, $\beta = \frac{\pi}{10}$ and $R_w = 2$.

[5] A. Eringen. Theory of micropolar fluids. *Tech. Rep.*, DTIC Document, 1965.

[6] M. Fakour, D. Ganji, M. Abbasi. Scrutiny of underdeveloped nanofluid mhd flow and heat conduction in a channel with porous walls. *Case Studies in Thermal Engineering*, 2014, **4**: 202–214.

[7] M. Fakour, A. Vahabzadeh, D. Ganji. Study of heat transfer and flow of nanofluid in permeable channel in the presence of magnetic field. *Propulsion and Power Research*, 2015, **4**(1): 50–62.

[8] M. Fakour, A. Vahabzadeh, et al. Analytical study of micropolar fluid flow and heat transfer in a channel with permeable walls. *Journal of Molecular Liquids*, 2015, **204**: 198–204.

[9] A. Kumar Gupt. Performance and analysis of blood flow through carotid artery. *International Journal of Engineering Business Management*, 2011, **3**(4): 1–6.

[10] B. Lee, S. Xue, et al. Determination of the blood viscosity and yield stress with a pressure-scanning capillary hemorheometer using constitutive models. *Korea-Australia Rheology Journal*, 2011, **23**(1): 1–6.

[11] A. Majidian, M. Fakour, A. Vahabzadeh. Analytical investigation of the laminar viscous flow in a semi-porous channel in the presence of a uniform magnetic field. *International Journal of Partial Differential Equations and Applications*, 2014, **2**(4): 79–85.

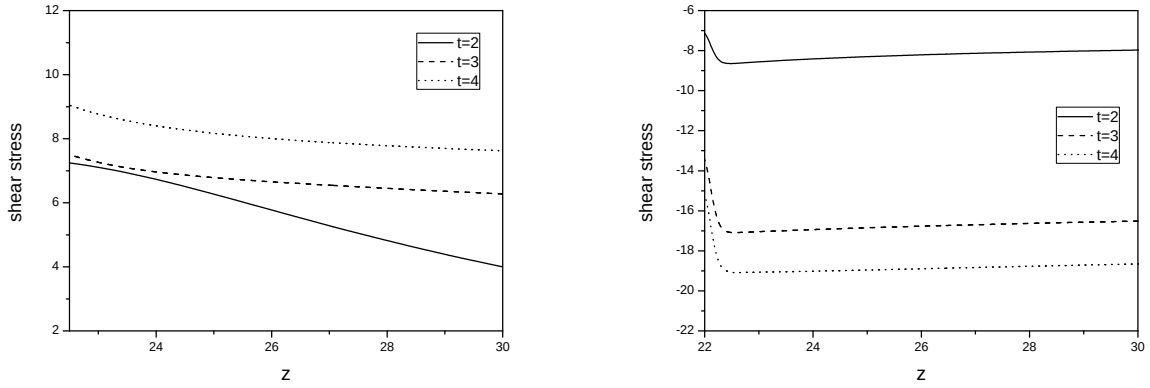

(a) (b)

Fig. 14: Influence of time on Shear stress along (a) the inner and (b) the outer walls of the daughter artery with fixed values of $H = 2$, $N = 0.75$, $m = 10$, $s = 1.5$, $G_r = 2$, $P_r = 0.7$, $\beta = \frac{\pi}{10}$ and $R_w = 2$.

[12] K. Mekheimer, M. Mohamed. Interaction of pulsatile flow on the peristaltic motion of a magneto-micropolar fluid through porous medium in a flexible channel: Blood flow model. *International Journal of Pure and Applied Mathematics*, 2014, **94**(3): 323.

[13] J. Misra, S. Chandra, et al. Electroosmotic oscillatory flow of micropolar fluid in microchannels: application to dynamics of blood flow in microfluidic devices. *Applied Mathematics and Mechanics*, 2014, **35**(6): 749–766.

[14] S. Nadeem, N. S. Akbar, et al. Power law fluid model for blood flow through a tapered artery with a stenosis. *Applied Mathematics and Computation*, 2011, **217**(17): 7108–7116.

[15] S. Nadeem, S. Ijaz. Theoretical analysis of metallic nanoparticles on blood flow through stenosed artery with permeable walls. *Physics Letters A*, 2015, **379**(6): 542–554.

[16] N. Nandakumar, K. Sahu, M. Anand. Pulsatile flow of a shear-thinning model for blood through a two-dimensional stenosed channel. *European Journal of Mechanics-B/Fluids*, 2015, **49**: 29–35.

[17] A. Nazir, M. Shafique. Numerical study of micropolar fluids flow due to a stretching cylinder by sor iterative procedure. 2015.

[18] R. Ponalagusamy, R. Selvi. Influence of magnetic field and heat transfer on two-phase fluid model for oscillatory blood flow in an arterial stenosis. *Meccanica*, 2015, **50**(4): 927–943.

[19] K. Ramesh, M. Devakar. Effects of heat and mass transfer on the peristaltic transport of mhd couple stress fluid through porous medium in a vertical asymmetric channel. *Journal of Fluids*, 2015, **2015**.

[20] J. Reddy, D. Srikanth. The polar fluid model for blood flow through a tapered artery with overlapping stenosis: Effects of catheter and velocity slip. *Applied Bionics and Biomechanics*, 2015, **2015**.

[21] G. Shit, M. Roy. Pulsatile flow and heat transfer of a magneto-micropolar fluid through a stenosed artery under the influence of body acceleration. *Journal of Mechanics in Medicine and Biology*, 2011, **11**(03): 643–661.

[22] N. Srivastava. Analysis of flow characteristics of the blood flowing through an inclined tapered porous artery with mild stenosis under the influence of an inclined magnetic field. *Journal of Biophysics*, 2014, **2014**.

[23] D. Tripathi, O. A. Bég, J. Curiel-Sosa. Homotopy semi-numerical simulation of peristaltic flow of generalised oldroyd-b fluids with slip effects. *Computer methods in biomechanics and biomedical engineering*, 2014, **17**(4): 433–442.